Multiresolution 3D-Computerized Tomography and its Application to NDT

Steven OECKL, Tobias SCHÖN, Fraunhofer EZRT, Fürth, Deutschland, Andreas KNAUF; Friedrich-Alexander-Universität., Erlangen, Deutschland, Alfred K. LOUIS, Universität des Saarlandes, Saarbrücken, Deutschland

Abstract. This paper presents a new approach for multiresolution reconstruction in 3D Feldkamp-type cone-beam tomography. The approximative inverse is used to derive an inversion formula for reconstructing the wavelet approximation and wavelet detail coefficients of the volume slice by slice. Beyond the reconstruction algorithm, applications of multiresolution reconstruction in the field of non-destructive testing are shown: The algorithm supports progressive reconstruction and local tomography for recovering only a region of interest inside the investigated volume. The features of the reconstruction algorithm are shown by means of simulation data as well as real data of an aluminium casting from automobile industry.

1. Introduction

Since wavelet analysis has become a powerful tool for signal and image processing, the multiresolution approach provides a solution for many practical applications. In X-ray computerized tomography algorithms for multiresolution 2D parallel beam, 2D fan-beam, and 3D cone-beam (Feldkamp-type) reconstruction using tensor or quincunx wavelets were introduced in [1,2,3]. These reconstruction formulas are based one the strong relationship between the continuous wavelet transform and the Radon transform as mentioned in [4]. In this paper we introduce a new approach to achieve an algorithm for reconstructing an object at different resolutions: The approximative inverse, see [5], is a method for solving first kind operator equations $Af = g$ in a stable way. Instead of determining the exact solution f, an inversion operator for f_e is calculated, where f_e is associated to f by $\langle f, e \rangle$ using a mollifier e. Applying the approximative inverse to computerized tomography yields a reconstruction algorithm of filtered backprojection type [6]. If we choose the mollifier as a wavelet, f_e represents the wavelet coefficients of f. For the sake of simplicity we introduce a nonseparable multiresolution inversion formula only for the 2D parallel scanning geometry. The resulting inversion formula using the approximative inverse is equal to the formula in [1]. In case of narrow cone-beam angles we make use of the Feldkamp algorithm [8]. We replace the standard ramp filter by the proposed ramp-wavelet filter, where the 2D multiresolution acts slice by slice.

In section 2 we provide the basic terminology of multiresolution analysis. A short introduction to the concept of the approximative inverse is given in section 3. The nonseparable multiresolution reconstruction algorithm using the approximative inverse is shown in section 4. Section 5 contains the results of the proposed algorithm. Finally a conclusion is given in section 6.

2. Multiresolution Analysis

The concept of multiresolution analysis (MRA) on $L^2(R)$ proposed in [7] is generalized to $L^2(R^2)$ using a dilation matrix $D \in Z^{2\times 2}$. Define $M := |\det D|$. A biorthogonal 2D-MRA requires a pair of dual scaling functions $\{\phi, \tilde{\phi}\}$ and $M-1$ pairs of dual mother wavelets $\{\psi^i, \tilde{\psi}^i\}$, $i = 1,\ldots,M-1$. For $j \in Z$, $k \in Z^2$, and $f \in L^2(R^2)$ we define the dilated and translated versions of f concerning D via

$$f_{j,k} := f_{j,k}^D := |\det D|^{-(j/2)} f(D^{-j}\cdot - k).$$

For a fixed $J \in Z$, the set $\{\phi_{J,k} : k \in Z^2\}$ is a frame for the approximation space $V_J \subset L^2(R^2)$. Let $W_J \subset L^2(R^2)$ be the complement of V_J in $V_{J-1} \subset L^2(R^2)$. Then the set $\{\psi^i_{J,k} : k \in Z^2, i = 1,\ldots,M-1\}$ is a frame for the detail space W_J. Therefore, every $f \in L^2(R^2)$ can be expanded in a wavelet series:

$$f = \sum_{k\in Z^2} \langle f, \phi_{J,k}\rangle \tilde{\phi}_{J,k} + \sum_{i=1}^{M-1}\sum_{j\le J}\sum_{k\in Z^2} \langle f, \psi^i_{j,k}\rangle \tilde{\psi}^i_{j,k} \ .$$

The coefficients $\langle f, \phi_{J,k}\rangle$ represent the discrete approximation of f at decomposition level J, whereas the wavelet coefficients $\langle f, \psi_{J,k}\rangle$ contain the details in which the discrete approximations of f at decomposition level J and $J-1$ are different. For the purpose of local tomography we are interested in reconstructing the approximation and detail coefficients directly from the projection data.

3. Approximative Inverse

In this section we give a short introduction to the concept of approximate inverse, for details see [5]. Let therefore be Ω a bounded subset of R^n and let $U := L^2(\Omega)$. Let V be a Hilbert space and let $A : U \to V$ be a linear, continuous operator. To determine for $f \in U$, $g \in V$ an approximative solution of $Af = g$, we use the following approach: For each $x \in \Omega$ define a mollifier $e_x \in U$ and an associated approximation

$$f_e(x) := \langle f, e_x\rangle_U .$$

Let A^* denote the adjoint operator of A. If there exists a $v_x \in V$ such that $A^* v_x = e_x$, we have

$$f_e(x) = \langle f, e_x\rangle_U = \langle f, A^* v_x\rangle_U = \langle Af, v_x\rangle_V = \langle g, v_x\rangle_V =: S_e g(x)$$

If $A^* v_x = e_x$ is not solvable, we minimize the defect by solving $AA^* v_x = Ae_x$ and define $S_e g(x) := \langle g, v_x\rangle_V$. We call the map $S : Y \to X$ the approximative inverse of A and v the

approximation kernel. The advantage of this approach is that the reconstruction kernel can be computed independently of the data. Furthermore, invariances and symmetries of the operator A can be transferred to S.

4. Reconstruction method

Let $\mathrm{S}(\mathrm{R}^n)$ denote the Schwartz space of rapidly decreasing functions on R^n and S^{n-1} the unit sphere in R^n. For $f \in S(R^n)$ and $w \in \mathrm{R}^n$ we define the Fourier transform

$$\hat{f}(w) := (2\pi)^{-n/2} \int_{\mathrm{R}^n} f(x) e^{-iwx} dx .$$

4.1. Radon transform

In this section we introduce some basic properties of the radon transform. A detailed overview can be found in [9]. For $f \in S(R^n)$, $\theta \in S^{n-1}$, and $s \in R$ the Radon transform is defined

$$Rf(\theta, s) := R_\theta f(s) := \int_{\theta^\perp} f(s\theta + t) dt .$$

The Fourier slice theorem shows the strong relationship between the Radon transform and the Fourier transform: For $\sigma \in \mathrm{R}$ we have

$$(R_\theta f)\hat{}(\sigma) = (2\pi)^{(n-1)/2} \hat{f}(\sigma\theta)$$

Let $g(\theta, s) := g_\theta(s) := R_\theta f$ be in the range of the radon transform and $x \in \mathrm{R}^n$. The adjoint operator of R has the form

$$R^* g(x) = \int_{S^{n-1}} g(\theta, x^{\mathrm{T}}\theta) d\theta$$

With $\alpha < n$, $w \in \mathrm{R}^n$ we define the Riesz potential

$$(I^\alpha f)\hat{}(w) := |w|^{-\alpha} \hat{f}(w)$$

Using the Riesz potential we are able to formulate the following inversion formula:

$$f = \frac{1}{2}(2\pi)^{1-n} R^* I^{1-n} g$$

where the Riesz potential acts on the second variable.

4.2 The approximative inverse of the Radon transform

We solve now the problem $Rf = g$ for $f \in \mathrm{S}(\mathrm{R}^2)$ using the approximative inverse. For $x \in \mathrm{R}^2$ and $e_x \in \mathrm{S}(\mathrm{R}^2)$ we define

$$v_x := \frac{1}{2}(2\pi)^{-1} I^{-1} R e_x$$

Then, due to the inversion formula for the Radon transform, v_x solves the equation $R^* v_x = e_x$ and is therefore the reconstruction kernel of the approximative inverse of the Radon transform. We have

$$\begin{aligned} f_e(x) &= S_e g(x) \\ &= \langle g, v_x \rangle_{\mathrm{S}(\mathrm{S}^1 \times \mathrm{R})} \\ &= \frac{1}{2}(2\pi)^{-1} \int_{\mathrm{S}^1} \int_{\mathrm{R}} g_\theta(s) I^{-1} R_\theta e_x(s)\, ds\, d\theta \\ &= \frac{1}{2}(2\pi)^{-1} \int_{\mathrm{S}^1} \int_{\mathrm{R}} I^{-1} g_\theta(s) R_\theta e_x(s)\, ds\, d\theta \end{aligned}$$

4.3 Reconstruction algorithm

For a fixed $J \in Z$ and $x \in \mathrm{R}^2$ we define the mollifier $e_x := \psi_{J,x}$. The approximative inverse has the form

$$f_e(x) = \langle f, e_x \rangle = \langle f, \psi_{j,x} \rangle$$

Hence the approximative inverse evaluated at $k \in Z^2$ is equal to the wavelet coefficient $\langle f, \psi_{j,k} \rangle$. To derive an inversion formula we define for $h \in S(R^n)$ and $y \in R^n$ the translation operator $T_y h := h(\cdot + y)$. Since $R_\theta T_y f = T_{\langle y,\theta \rangle} R_\theta f$ and $R_\theta \psi_{J,x} = R_\theta \psi_{J,0}(\cdot - D^J x)$ we conclude

$$\begin{aligned} f_e(k) &= S_e g(k) \\ &= \frac{1}{2}(2\pi)^{-1} \int_{\mathrm{S}^1} \int_{\mathrm{R}} I^{-1} g_\theta(s) R_\theta \psi_{J,k}(s)\, ds\, d\theta \\ &= \frac{1}{2}(2\pi)^{-1} \int_{\mathrm{S}^1} \int_{\mathrm{R}} I^{-1} g_\theta(s) R_{-\theta} \psi_{J,0}(\langle D^J k, \theta \rangle - s)\, ds\, d\theta \\ &= \frac{1}{2}(2\pi)^{-1} R^*(I^{-1} g_\theta * R_{-\theta} \psi_{J,0})(D^J k) \end{aligned}$$

The inversion formula is of filtered backprojection type and leads therefore to a fast implementation. We are able to formulate an inversion formula to reconstruct the approximation coefficients $\langle f, \phi_{j,k} \rangle$ in the same way.

5. Results

We have used a multiresolution analysis with quincunx decimation, i.e. the dilation matrix was defined $D := (1\,1;1\,-1)$. Starting with a pair of 1D biorthogonal filters, we have used the McClellan transform [10] to generate 2D nonseparable diamond shaped filters. The near coiflet wavelet with five coefficients [11, Table III] was implemented to create our results due to its good localization property concerning the Radon transform [3]. Figure 1 shows the 2D near coiflet scaling and wavelet filter created via the McClellan transform.

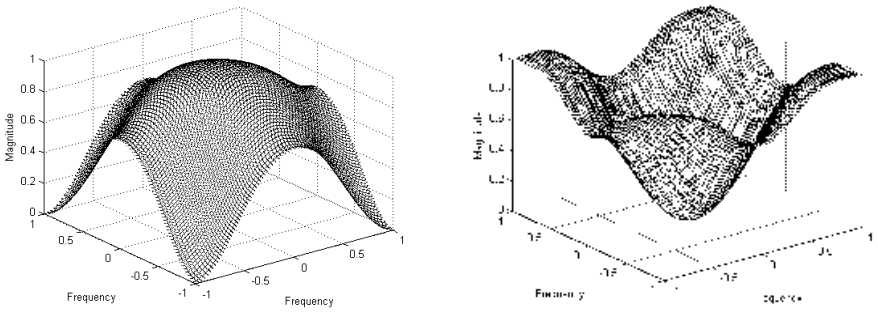

a) b)

Fig. 1: 2D near coiflet filter created via McClellan transform. a) scaling filter. b) wavelet filter.

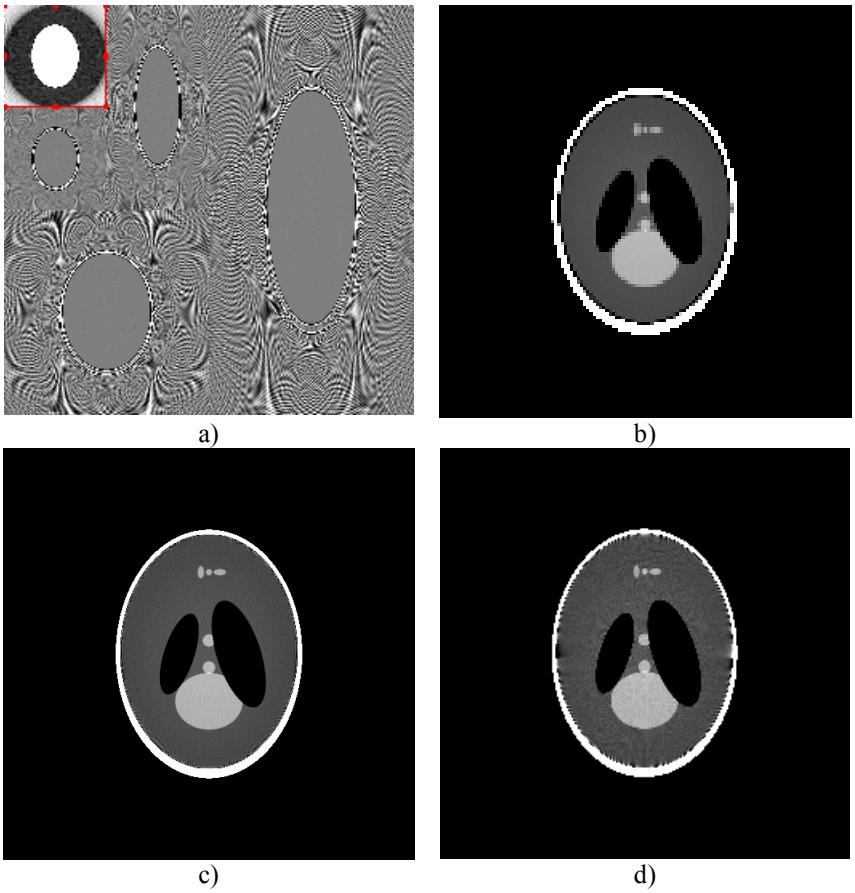

a) b)

c) d)

Fig. 2: Fan-beam reconstruction: a) Approximation and detail coefficients at decomposition level 4 using the proposed reconstruction method. b) Zoomed approximation coefficients from selected region in a). c) Synthesis of coefficients in a). d) Reconstruction using ramp filtered backprojection.

The proposed algorithm for 2D reconstruction was applied to simulated fan-beam projections of the Shepp-Logan phantom. The reconstruction was performed on a 512×512

pixel grid using 400 projection with 512 detector pixels equidistantly spaced on $[0,2\pi]$ and fan-beam angle $14{,}6^\circ$. Figure 2 shows the results of the proposed reconstruction method and a comparison with the standard filtered backprojection using ramp filtering. The approximation and detail coefficients in figure 2a) are displayed in the contrast range $[-0.27;0.27]$, whereas in figure 2b)-d) we have used the range $[1.0;1.026]$.

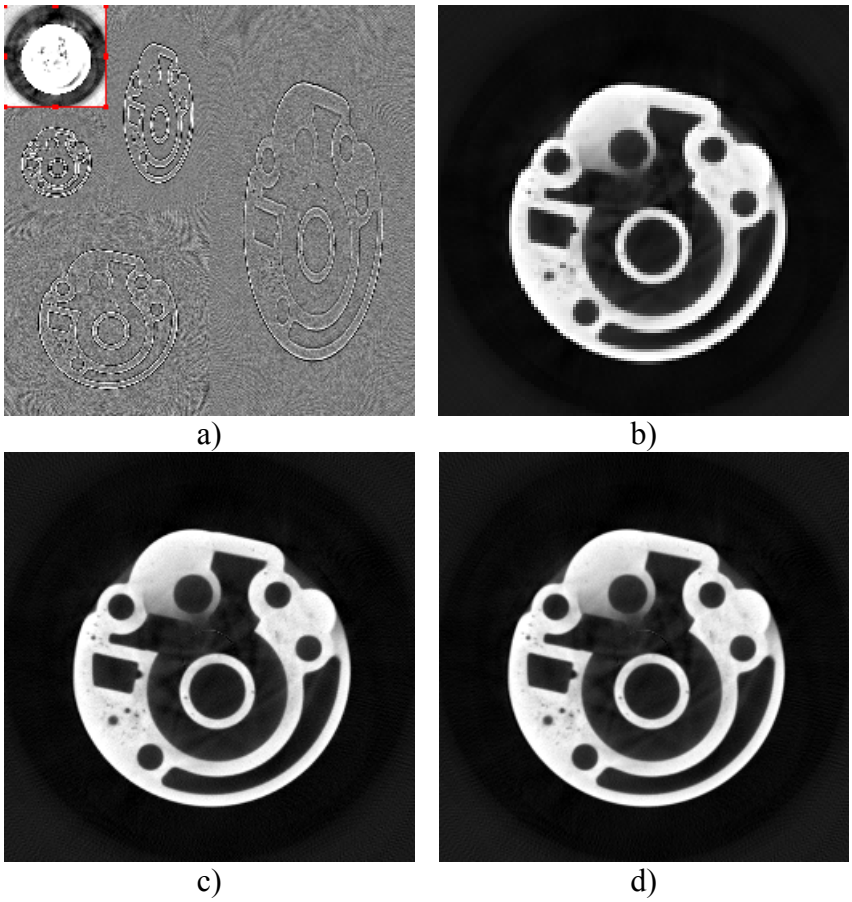

Fig. 3: Feldkamp-type cone beam reconstruction of a decentralized slice: a) Approximation and detail coefficients at decomposition level 4 using the proposed reconstruction method. b) Zoomed approximation coefficients from selected region in a). c) Synthesis of coefficients in a). d) Reconstruction using ramp filtered backprojection.

Figure 3 illustrates the results of a Feldkamp-type cone beam reconstruction with the proposed ramp-wavelet filtering using real data of an aluminium casting The reconstruction was performed on a $512\times512\times181$ voxel grid using 400 flat panel detector projections with 512×512 pixels equidistantly spaced on $[0,2\pi]$ and cone beam angle $6{,}8^\circ$. The approximation and detail coefficients in figure 3a) are displayed in the contrast range $[-0.27;0.27]$, whereas in figure 3b)-d) we have used the range $[0.0;5.89]$.

For practical applications the possibility to perform a progressive reconstruction is the main advantage of multiresolution tomographic reconstruction. Reconstructing the approximation coefficients at a high decomposition level yields a first impression of the specimen. After selecting a region of interest within the approximation only the detail coefficients of the selected region plus a certain border must be reconstructed to achieve high resolution inside the region of interest. Figure 4 shows an example using again the aluminium casting from figure 3. Figure 4a) shows the approximation coefficients at decomposition level four and the detail coefficients of a selected region of interest. Performing a synthesis using only these detail coefficients yields high resolution inside the region of interest and a coarse reconstruction elsewhere, see figure 4b). A zoomed version

of the locally reconstructed region of interest and the corresponding region of a ramp filtered backprojection can be seen in figure 4c)-d). The contrast ranges in figure 4 are the same as in figure 3.

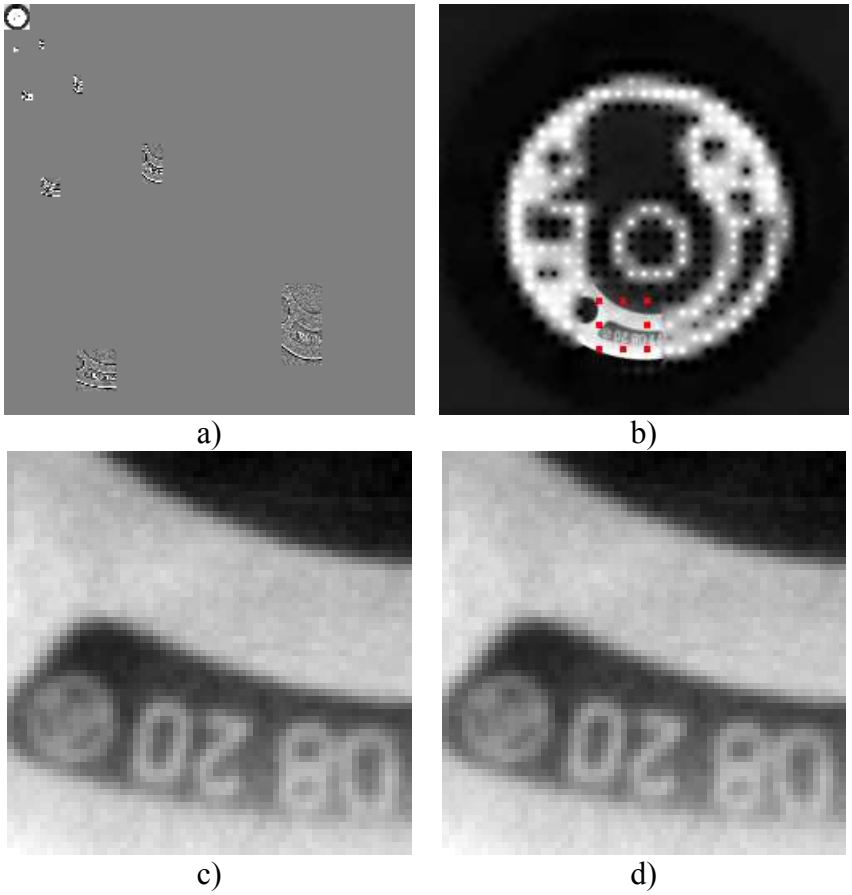

Fig. 4: Local Feldkamp-type cone beam reconstruction inside of a decentralized slice: a) Approximation and selected detail coefficients at decomposition level 4 using the proposed reconstruction method. b) Synthesis using the coefficients in a). c) Zoomed region of interest as selected in b). d) Corresponding region of interest inside of a ramp filtered backprojection.

6. Conclusion

We have proposed an inversion formula for nonseparable multiresolution tomographic reconstruction using the approximative inverse. Applying the approximative inverse to computerized tomography yields a family of inversion formulas. We have shown that nonseparable multiresolution tomographic reconstruction is a special case within this family of inversion formulas. A synthesis of the calculated approximation and detail coefficients yields a reconstruction image that differs only slightly from the associated ramp filtered backprojection image. We have illustrated that the progressive reconstruction feature makes the proposed method useful for practical applications, for example local tomography.

References

[1] S. Bonnet, F. Peyrin, F. Turjman, and R. Prost. Multiresolution Reconstruction in Fan-Beam Tomography. IEEE Transactions on Image Processing, 11(3), 169-176, March, 2002.

[2] S. Bonnet, F. Peyrin, F. Turjman, and R. Prost. Nonseparable Wavelet-Based Cone-Beam Reconstruction in 3-D Rotational Angiography. IEEE Transactions on Medical Imaging, 22(3), 360-367, March, 2003.

[3] F. Rashid-Farrokhi, K. J. Ray Liu, C. A. Berenstein, and D. Walnut. Wavelet-Based Multiresolution Local Tomography. IEEE Transactions on Image Processing, 6(10), 1412-1430, October, 1997.

[4] D. Walnut. Applications of Gabor and wavelet expansions to the Radon transform. In J. S. Byrnes et al, editor, Probabilistic and Stochastic Methods in Analysis, With Applications, pages 187-205, Kluwer Academic Publishers, 1992.

[5] A. K. Louis. Approximate inverse for linear and some nonlinear problems. Inverse Problems, 12, 175-190, 1996.

[6] A. K. Louis. Filter design in three-dimensional cone beam tomography: circular scanning geometry. Inverse Problems, 19, 31-40, 2003.

[7] S. Mallat. A theory for multiresolution signal decomposition: The wavelet representation. IEEE Transactions on Pattern Analysis and Machine Intelligence, 11, 674-693, July, 1989.

[8] L. A. Feldkamp, L. C. Davis, and J. W. Kress. Practical cone-beam algorithm. J. Opt. Soc. Am. A, 1(6), 612-619, June, 1984.

[9] F. Natterer. The Mathematics of Computerized Tomography. John Wiley & Sons, 1986.

[10] J. H. McClellan. The design of two-dimensional digital filters by transformations. Proc. 7th Annu. Princeton Conf. Information Science Systems, 247-251, 1973.

[11] M. Antonini, M. Barlaud, P. Mathieu , and I. Daubechies. Image Coding Using Wavelet Transform. IEEE Transactions on Image Processing, 1(2), 205-220, April, 1992.